Shape-Controlled Second-Harmonic Scattering from Gold Nano-Tetrapods

Jieli Lyu, Fabien Rondepierre, Christian Jonin, Pierre-François Brevet, Cyrille Hamon, Doru Constantin

Shape-Controlled Second-Harmonic Scattering from Gold Nano-Tetrapods

Jieli Lyu,[†] Fabien Rondepierre,[‡] Christian Jonin,[‡] Pierre-François Brevet,[*,‡] Cyrille Hamon,[*,†] and Doru Constantin[*,¶]

[†]*Université Paris-Saclay, CNRS, Laboratoire de Physique des Solides, 91405 Orsay, France*

[‡]*Institut Lumière Matière, UMR 5306 CNRS and Université Claude Bernard Lyon 1, F-69622 Villeurbanne, France*

[¶]*Institut Charles Sadron, CNRS and Université de Strasbourg, 67034 Strasbourg, France*

E-mail: pfbrevet@univ-lyon1.fr; cyrille.hamon@universite-paris-saclay.fr; constantin@unistra.fr

Abstract

In the search for efficient building blocks for nonlinear metamaterials, plasmonic nanoparticles have received considerable attention. Their quadratic nonlinear optical properties result from a complex interplay between the nature of the bulk material, the object shape, surface defects and retardation effects. This versatility can be used to tailor the properties of the resulting material. However, despite extensive investigation, separating and controlling these contributions is still a challenge. In this report, we control the morphology of colloidal gold nanoparticles with tetrahedral symmetry and explore their second harmonic scattering response. The material itself is centrosymmetric but not the shape, conferring to the first hyperpolarizability an almost purely octupolar symmetry. Gradually reshaping the nanoparticles into spheres (and thus decreasing their asymmetry) reduces their nonlinear response, showing that it is is controlled by the morphology. These results open the way towards new kinds of nonlinear plasmonics platforms and imaging probes.

Keywords

Au nanoparticles, nonlinear optics, hyperpolarizability, symmetry

Introduction

The design of novel materials aiming for full control of the light-matter interaction (such as metamaterials and metasurfaces) has been largely driven by the development of nanoscale structures, using either top-down or bottom-up methods. Among the latter, the use of colloidal building blocks with optical properties defined during the synthesis step has been very fruitful. However, the influence of the various relevant parameters (shape, size, surface roughness, etc.) is difficult to discriminate and adjust separately.

Gold nanoparticles (NPs) display exciting linear optical properties, notably due to the existence of well-defined localized surface plasmon resonances, very sensitive to the morphology of the particles.[1] This dependence has been explored in detail and has led to successful applications. It is thus a natural step to extend this study to the NPs' nonlinear response. However, since gold is centrosymmetric, the bulk contribution vanishes altogether under homogeneous excitation and the SHG is then due to the particle shape (provided it is non-centrosymmetric itself),[2] to surface defects –notably due to coatings– and, for NPs large enough with respect to the wavelength, to retardation contributions (the non-vanishing spatial phase of the excitation field over the volume of the object[3,4]) or to the presence of a substrate, which breaks the inversion symmetry.[5] Separating these various effects is a real challenge and requires the use of NPs with well-controlled morphology and low surface roughness. Significant progress has been made in the lithographic fabrication of non-centrosymmetric gold NPs,[6,7] but in this approach the substrate must also be taken into account, making the analysis difficult. The chemical synthesis of such nano-objects is still under development, although a large range of shapes and sizes have been proposed.[8]

Yet, aside from nanoprisms, the synthesis of non-centrosymmetric shapes is less developed than for centrosymmetric ones like spheres, cubes or rods. Nevertheless, obtaining these NPs with different shapes via a bottom-up procedure would have many advantages: large yield, smooth surfaces, the absence of a substrate and the possibility of using them as tracers, e.g. in nonlinear microscopy.

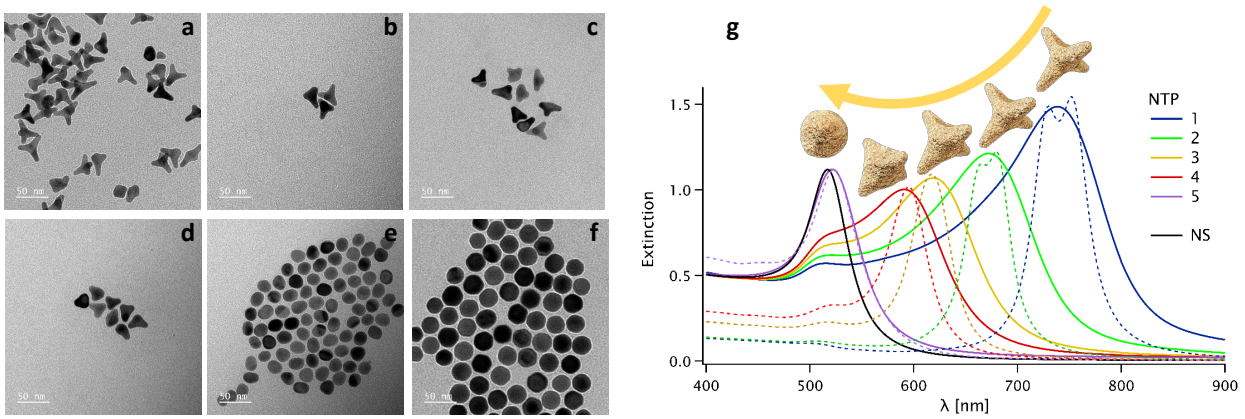

Figure 1: TEM images of: (a-e) NTPs obtained after various reshaping times: 3 min., 18 min., 33 min., 48 min. and 12 h, (f) NS, and (g) UV-Vis spectra of particle suspensions, renormalized to an extinction of 0.5 at $\lambda = 400\,\mathrm{nm}$ (solid lines) and spectra of the model shapes, simulated using BEM (dashed lines). The NTPs are represented above each curve.

Fundamentally, the SHG response from NPs is described by the third-rank first hyperpolarizability tensor β, which can be irreducibly decomposed into a dipolar $\beta^{(1)}$ and an octupolar $\beta^{(3)}$ contribution. When the material itself is centrosymmetric, one can break the overall symmetry by rendering the objects dipolar, e.g. by creating a preferential axis and introducing an asymmetry along this direction. This approach has been attempted, for instance, with heterogeneous NP dimers.[9–11] Another possibility is to develop the octupolar $\beta^{(3)}$ component with a three-fold symmetry, while maintaining a low dipole.[12] This has been done for lithographed nanoprism arrangements with D3h symmetry[13,14] and for colloidal nanoprisms in solution.[15] Obtaining materials with an octupolar response is interesting,[16,17] both from a fundamental point of view and for applications, since the SHG intensity has a very characteristic polarization pattern.

In this work, we achieve two objectives: controlling the morphology of gold nano-

tetrapods (NTPs), a shape first obtained with semiconductors,[18] and showing that their nonlinear optical response has an octupolar structure. These objects feature four arms with almost perfect tetrahedral Td symmetry and have recently been obtained with high yield.[19] Their morphology is very promising for nonlinear optics (and for SHG in particular), as they should have a vanishing $\beta^{(1)}$ and a large $\beta^{(3)}$. Their small size offers the opportunity to study the SHG response of low-symmetry nanostructures without retardation effects. Such studies can be conveniently performed at the ensemble level due to their narrow size distribution. Moreover, the NTP is a metastable shape, which reforms into a sphere over a few hours (see Figure 1). We have discovered that coating the NTPs with a thin silver layer blocks the reshaping process. This feature enables us to study a family of NPs with varying arm length while keeping the volume constant, and thus to follow the balance between the sources of their SHG response (in particular, the $\beta^{(1)}/\beta^{(3)}$ ratio). This family of particles opens the way towards colloidally assembled nonlinear plasmonics platforms.

Methods

Gold NTPs were synthesized following the method of Chang et al.[19] We applied a thin silver layer at an Ag/Au molar ratio of 0.2 at different times after particle formation, obtaining nano-objects with the same total volume, but various arm lengths L and core diameters $2R$, as shown in Figure 1a-e. Gold nano-spheres (NS) were prepared by two growth steps onto monocrystalline seeds.[20] After synthesis they were also covered with silver (Ag/Au= 0.2), an operation that does not change the morphology of the particles[21] (see Figure 1f). The thickness of the silver layer is below one nanometer (we estimate it as 0.5 nm for NTP1, increasing to 0.66 nm for NTP5, due to the reshaping changing the area-to-volume ratio.) Since the SH signal is clearly dominated by the overall particle symmetry, we do not expect the D and ζ^V parameters to be affected by the silver layer, which might however increase slightly the hyperpolarizability β, as silver is known to provide a higher response than gold.[22]

All particles were dispersed in an aqueous solution of 10 mM cetyltrimethylammonium chloride (CTAC), at an Au^0 concentration of 0.17 mM (NTPs) or 0.22 mM (NS). Their dimensions are given in Table 1 and their UV-Vis extinction spectra are displayed in Figure 1g, along with boundary element method (BEM) simulations. All objects display a plasmon band centered around 520 nm, typical for small gold nanoparticles in water, as well as a second band, whose strength and red shift with respect to the first one are proportional to the arm length. By analogy with the case of nanorods, we will label these bands as "transverse" and "longitudinal", respectively.

Table 1: Particle sizes extracted from the TEM images (mean value ± SD): arm length L and core diameter $2R$ for the NTPs, diameter $2R$ for the NS. Simulation parameters: BEM simulations were done using the TEM values for $2R$ and the slightly higher values L_{BEM} for the arm length in order to yield good agreement between the fits and the data in Figure 1g (see the Supporting Information for more details). HRS parameters: first hyperpolarizability β, depolarization ratio D and retardation parameter ζ^V (see the text for details).

Sample	Age	L [nm]	$2R$ [nm]	L_{BEM} [nm]	$\beta[10^{-25}\,\mathrm{esu}]$	D	ζ^V
NTP-1	3 min.	17.1 ± 2.3	15.2 ± 1	19	6.04 ± 0.06	0.61 ± 0.01	0.01 ± 0.002
NTP-2	18 min.	11.1 ± 2.6	15.8 ± 0.8	13	2.56 ± 0.03	0.52 ± 0.02	$(4 \pm 0.5)\,10^{-3}$
NTP-3	33 min.	8.7 ± 2.3	16.6 ± 0.8	9.5	1.42 ± 0.11	0.48 ± 0.01	0.13 ± 0.01
NTP-4	48 min.	6.3 ± 2.2	17.0 ± 0.6	7.5	1.3 ± 0.09	0.38 ± 0.01	0.11 ± 0.01
NTP-5	12 h.	0	19.6 ± 1.2	0	1.5 ± 0.17	0.20 ± 0.01	0.08 ± 0.01
NS	–	–	28.1 ± 2.1	–	0.56 ± 0.05	0.27 ± 0.01	0.33 ± 0.06

The hyper Rayleigh scattering (HRS)[23] setup has been described elsewhere.[24] It comprises a mode-locked Ti:sapphire laser tuned to 800 nm and delivering pulses of about 180 fs at a repetition rate of 80 MHz. The mean power was set at about 450 mW at the sample level to avoid any heating or deterioration as checked by simple extinction spectroscopy of the sample cell before and after each measurements. The fundamental laser beam was focused with a 16× objective (NA 0.32) into a quartz cell with 5 mm-long optical path (Q107 cell, Hellma). The intensity I_{HRS} scattered at a right angle from the incident beam was collected with a lens and sent to a spectrometer coupled to a cooled CCD camera. Color filters were inserted to remove any unwanted harmonic light before the cell and fundamental light after the cell.

The linear polarization of the fundamental beam was controlled with a half-wave plate, defining the angle γ with respect to the laboratory vertical direction. The polarization angle Γ of the harmonic light was selected with a linear polarizer placed either vertically ($\Gamma = 0$) or horizontally ($\Gamma = \pi/2$), denoted in the following by V and H, respectively. For the two Γ position, we measured $I^{\Gamma}_{\mathrm{HRS}}(\gamma)$ over a complete 2π range in γ, see e.g. Figure 2 top. The concentration dependence of $I^{V}_{\mathrm{HRS}}(\gamma = 0)$ normalized to the solvent signal yielded the first hyperpolarizability β in absolute esu units using water as the reference while the dependence of the signal intensity on the polarization angle (Figure 2 bottom) yielded the depolarization ratio D[25] and the retardation parameter ζ^{V}, as detailed in the Supporting Information. All these quantities are given in Table 1 for each sample.

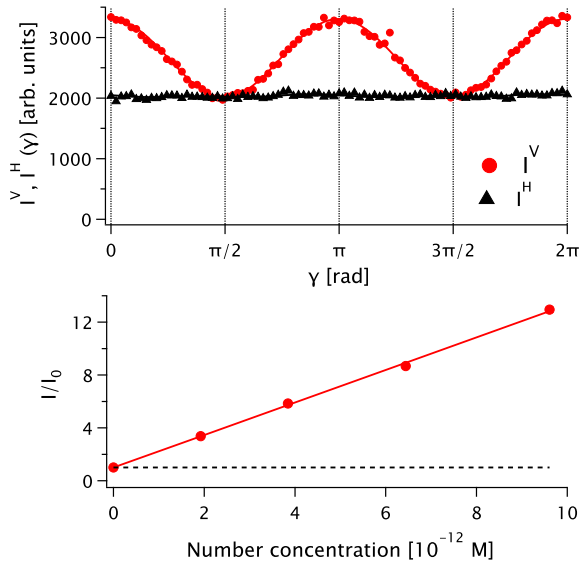

Figure 2: Sample NTP-1. Top: Polar graph of the (red) vertically and (black) horizontally polarized HRS intensity $I^{\Gamma}_{\mathrm{HRS}}(\gamma)$ as a function of the fundamental polarization angle (symbols) and fits (lines). Bottom: dilution law for the same sample. The signal $I^{V}_{\mathrm{HRS}}(\gamma = 0)$ is normalized to the solvent signal I_0. The slope of its dependence with respect to the particle concentration yields the first hyperpolarizability β.

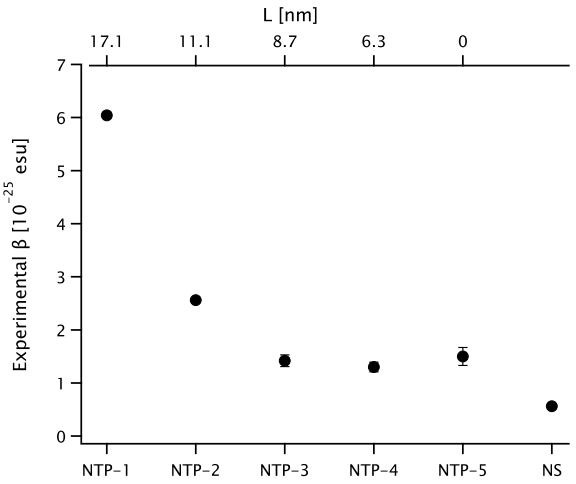

Figure 3: Left axis: first hyperpolarizability β for all the samples, identified on the bottom axis (solid black dots). Error bars are smaller than the symbol size. For NTPs, the arm length L is given on the top axis.

Results and Discussion

The first hyperpolarizability β (solid dots in Figure 3) decreases markedly as the NTPs reshape. The initial NTPs (sample NTP-1) have a hyperpolarizability β over 10 times higher than that of the reference nanospheres (sample NS), although their volume is three times lower! For the more symmetric shapes (NTP-3 to 5) β reaches a plateau of the order of 10^{-25} esu that we attribute to surface defects (leading to effective asphericity).

More information can be gleaned from the polarization dependence of $I^{\Gamma}_{\mathrm{HRS}}(\gamma)$. The depolarization ratio D (Figure 4, left) is initially rather high ($D = 0.61$), indicating a harmonic response with almost purely three-dimensional octupolar symmetry ($D_{\mathrm{oct}} = 2/3$), as expected from the shape of the NTPs. This parameter decreases along the reshaping process, spanning the range from D_{oct} to $D_{\mathrm{dip}} = 1/9$ for purely dipolar symmetry. The retardation parameter ζ^V (Figure 4, right) remains low for all samples, as expected for objects much smaller than the wavelength. For spheres (NS), where the shape is perfectly centrosymmetric and the surface free from defects, the only source of SHG is retardation, hence a high ζ^V value. This contribution is however ineffective at such small sizes, and

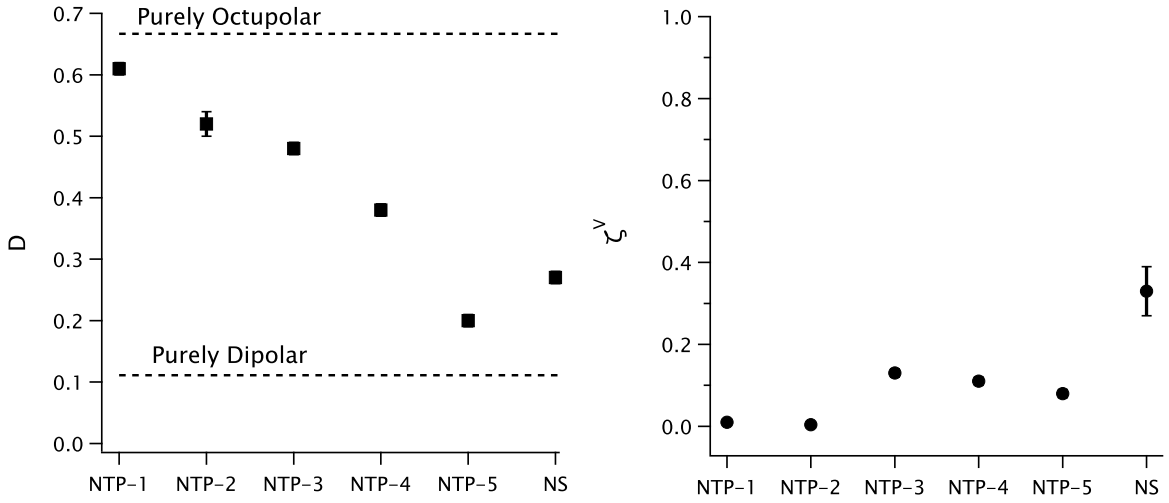

Figure 4: Depolarization ratio D (left) and retardation parameter ζ^V (right) for all the samples.

therefore the NS hyperpolarizability, the origin of which stems from the deviation of the NS shape from that of perfectly centrosymmetric spherical shape, is small. Deviation from the perfect spherical shape arise from geometrical defects as well as local surface defects like presence of adsorbates, silver layer defects, etc.. The determination of a depolarization ratio D is, in this context, a measure of the distribution of the defects at the nanoparticle surface, since it is indefinite for a pure retardation contribution (D being the ratio of two vanishing intensities). The experimental value, markedly different from the pure dipolar 1/9 theoretical value, indicates a rather general defect distribution over the entire surface. Therefore, from the observed experimental values of the D and ζ^V coefficients it is shown that, initially, retardation is weak and the SHG response dominated by the shape non-centrosymmetry, whereas as the NTPs evolve into spheres, this source of nonlinearity weakens and that originating in retardation takes a stronger weight.

Conclusions

In conclusion, gold nano-tetrapods exhibit strong SHG, essentially due to their shape (and hence with the same octupolar symmetry as the objects themselves) and which decreases as they reshape into spheres, reaching a plateau, the origin of which is driven by the surface defects. Initially, retardation is weak and the SHG response is dominated by the shape non-centrosymmetry. As the NTPs evolve into spheres, this source weakens and is complemented with an origin due to retardation.

The arm length (and hence the extinction spectrum) of the NTPs can be tuned over a wide range, which is very interesting in view of applications. For example, one could place either the maximum value (peak) or the steepest slope of the longitudinal plasmon band at the excitation frequency for maximum efficacy or sensitivity, respectively. The presence of two plasmon bands opens the way towards doubly resonant systems,[26] where the fundamental and harmonic frequencies coincide with the longitudinal and transverse bands, respectively.

The nanoparticle tips provide privileged spatial regions of high electromagnetic field enhancement, and are therefore highly sensitive to the local environment, an essential feature in sensing. The specific polarization pattern could also help discriminate the signal of the particles (or of molecules adsorbed to the particle tips) from parasitic contributions with a dipolar character, such as those due to the various interfaces in the system.

Possible applications to nonlinear imaging can also be envisioned, since the SHG signal is spectrally sharp and coherent, in contrast with two-photon luminescence, for instance. These advantages have already prompted the use of ferroelectric materials (e.g. $BaTiO_3$) as microscopy probes.[27,28] Gold nanoparticles have the added benefit of very versatile surface chemistry, making them adaptable to practically all relevant media (biological or otherwise).

Acknowledgement

J. L. acknowledges financial support by the China Scholarship Council (CSC). We thank

Claire Goldmann for the preparation of some nanoparticle batches and for continuous experimental support. The present work has benefited from the electronic microscopy facility of Imagerie-Gif, (http://www.i2bc.paris-saclay.fr), a member of IBiSA (http://www.ibisa.net), supported by "France-BioImaging" (ANR-10-INBS-04-01) and the Labex "Saclay Plant Science" (ANR-11-IDEX-0003-02).

Supporting Information Available

Nanoparticle synthesis, TEM images, details on the TEM, UV-Vis and HRS methods.

References

(1) Quinten, M. *Optical Properties of Nanoparticle Systems: Mie and Beyond*; Wiley-VCH: Weinheim, 2010.

(2) Finazzi, M.; Biagioni, P.; Celebrano, M.; Duò, L. Selection Rules for Second-Harmonic Generation in Nanoparticles. *Phys. Rev. B* **2007**, *76*, 125414.

(3) Butet, J.; Brevet, P.-F.; Martin, O. J. F. Optical Second Harmonic Generation in Plasmonic Nanostructures: From Fundamental Principles to Advanced Applications. *ACS Nano* **2015**, *9*, 10545–10562.

(4) Bonacina, L.; Brevet, P.-F.; Finazzi, M.; Celebrano, M. Harmonic Generation at the Nanoscale. *J. Appl. Phys.* **2020**, *127*, 230901.

(5) Zeng, Y.; Qian, H.; Rozin, M. J.; Liu, Z.; Tao, A. R. Enhanced Second Harmonic Generation in Double-Resonance Colloidal Metasurfaces. *Adv. Funct. Mater.* **2018**, *28*, 1803019.

(6) Cui, B.; Clime, L.; Li, K.; Veres, T. Fabrication of Large Area Nanoprism Arrays and

Their Application for Surface Enhanced Raman Spectroscopy. *Nanotechnology* **2008**, *19*, 145302.

(7) Valev, V. K.; Silhanek, A. V.; Verellen, N.; Gillijns, W.; Van Dorpe, P.; Aktsipetrov, O. A.; Vandenbosch, G. A. E.; Moshchalkov, V. V.; Verbiest, T. Asymmetric Optical Second-Harmonic Generation from Chiral G-Shaped Gold Nanostructures. *Phys. Rev. Lett.* **2010**, *104*, 127401.

(8) Shi, Y.; Lyu, Z.; Zhao, M.; Chen, R.; Nguyen, Q. N.; Xia, Y. Noble-Metal Nanocrystals with Controlled Shapes for Catalytic and Electrocatalytic Applications. *Chem. Rev.* **2021**, *121*, 649–735.

(9) Bachelier, G.; Russier-Antoine, I.; Benichou, E.; Jonin, C.; Del Fatti, N.; Vallée, F.; Brevet, P.-F. Fano Profiles Induced by Near-Field Coupling in Heterogeneous Dimers of Gold and Silver Nanoparticles. *Phys. Rev. Lett.* **2008**, *101*, 197401.

(10) Zielinski, M.; Winter, S.; Kolkowski, R.; Nogues, C.; Oron, D.; Zyss, J.; Chauvat, D. Nanoengineering the Second Order Susceptibility in Semiconductor Quantum Dot Heterostructures. *Opt. Express* **2011**, *19*, 6657–6670.

(11) Wang, J.; Butet, J.; Bernasconi, G. D.; Baudrion, A.-L.; Lévêque, G.; Horrer, A.; Horneber, A.; Martin, O. J. F.; Meixner, A. J.; Fleischer, M. et al. Strong Second-Harmonic Generation from Au-Al Heterodimers. *Nanoscale* **2019**, *11*, 23475–23481.

(12) Zyss, J. Molecular Engineering Implications of Rotational Invariance in Quadratic Nonlinear Optics: From Dipolar to Octupolar Molecules and Materials. *J. Chem. Phys.* **1993**, *98*, 6583–6599.

(13) Kolkowski, R.; Petti, L.; Rippa, M.; Lafargue, C.; Zyss, J. Octupolar Plasmonic Meta-Molecules for Nonlinear Chiral Watermarking at Subwavelength Scale. *ACS Photonics* **2015**, *2*, 899–906.

(14) Hou, R.; Shynkar, V.; Lafargue, C.; Kolkowski, R.; Zyss, J.; Lagugné-Labarthet, F. Second Harmonic Generation from Gold Meta-Molecules with Three-Fold Symmetry. *Phys. Chem. Chem. Phys.* **2016**, *18*, 7956–7965.

(15) Nadolski, K.; Benichou, E.; Tarnowicz-Staniak, N.; Żak, A.; Jonin, C.; Matczyszyn, K.; Brevet, P.-F. Adverse Role of Shape and Size in Second-Harmonic Scattering from Gold Nanoprisms. *J. Phys. Chem. C* **2020**, *124*, 14797–14803.

(16) Jeong, M.-Y.; Brasselet, S.; Lim, T.-K.; Cho, B. R. Octupolar Films with Large Second Harmonic Generation and Electro-Optical Effects. *Adv. Funct. Mater.* **2012**, *22*, 788–796.

(17) Khan, A. R.; Zhang, L.; Ishfaq, K.; Ikram, A.; Yildrim, T.; Liu, B.; Rahman, S.; Lu, Y. Optical Harmonic Generation in 2D Materials. *Adv. Funct. Mater.* **2022**, *32*, 2105259.

(18) Manna, L.; Milliron, D. J.; Meisel, A.; Scher, E. C.; Alivisatos, A. P. Controlled Growth of Tetrapod-Branched Inorganic Nanocrystals. *Nat. Mater.* **2003**, *2*, 382–385.

(19) Chang, Y.-X.; Zhang, N.-N.; Xing, Y.-C.; Zhang, Q.; Oh, A.; Gao, H.-M.; Zhu, Y.; Baik, H.; Kim, B.; Yang, Y. et al. Gold Nanotetrapods with Unique Topological Structure and Ultranarrow Plasmonic Band as Multifunctional Therapeutic Agents. *J. Phys. Chem. Lett.* **2019**, *10*, 4505–4510.

(20) Hanske, C.; González-Rubio, G.; Hamon, C.; Formentín, P.; Modin, E.; Chuvilin, A.; Guerrero-Martínez, A.; Marsal, L. F.; Liz-Marzán, L. M. Large-Scale Plasmonic Pyramidal Supercrystals via Templated Self-Assembly of Monodisperse Gold Nanospheres. *J. Phys. Chem. C* **2017**, *121*, 10899–10906.

(21) Lyu, J.; Geertsen, V.; Hamon, C.; Constantin, D. Determining the Morphology and Concentration of CoreShell Au/Ag Nanoparticles. *Nanoscale Adv.* **2020**, *2*, 4522–4528.

(22) Russier-Antoine, I.; Benichou, E.; Bachelier, G.; Jonin, C.; Brevet, P. F. Multipolar Contributions of the Second Harmonic Generation from Silver and Gold Nanoparticles. *J. Phys. Chem. C* **2007**, *111*, 9044–9048.

(23) Hendrickx, E.; Clays, K.; Persoons, A. Hyper-Rayleigh Scattering in Isotropic Solution. *Acc. Chem. Res.* **1998**, *31*, 675–683.

(24) Russier-Antoine, I.; Lee, H. J.; Wark, A. W.; Butet, J.; Benichou, E.; Jonin, C.; Martin, O. J. F.; Brevet, P.-F. Second Harmonic Scattering from Silver Nanocubes. *J. Phys. Chem. C* **2018**, *122*, 17447–17455.

(25) Brasselet, S.; Zyss, J. Multipolar Molecules and Multipolar Fields: Probing and Controlling the Tensorial Nature of Nonlinear Molecular Media. *J. Opt. Soc. Am. B* **1998**, *15*, 257.

(26) Gennaro, S. D.; Rahmani, M.; Giannini, V.; Aouani, H.; Sidiropoulos, T. P. H.; Navarro-Cía, M.; Maier, S. A.; Oulton, R. F. The Interplay of Symmetry and Scattering Phase in Second Harmonic Generation from Gold Nanoantennas. *Nano Lett.* **2016**, *16*, 5278–5285.

(27) Pantazis, P.; Maloney, J.; Wu, D.; Fraser, S. E. Second Harmonic Generating (SHG) Nanoprobes for in Vivo Imaging. *Proc. Natl. Acad. Sci. U.S.A.* **2010**, *107*, 14535–14540.

(28) Malkinson, G.; Mahou, P.; Chaudan, É.; Gacoin, T.; Sonay, A. Y.; Pantazis, P.; Beaurepaire, E.; Supatto, W. Fast In Vivo Imaging of SHG Nanoprobes with Multiphoton Light-Sheet Microscopy. *ACS Photonics* **2020**, *7*, 1036–1049.

Graphical TOC Entry